Bridging the gap between the Jaynes-Cummings and Rabi models using an intermediate rotating wave approximation

Yimin Wang[1,2], Jing Yan Haw[2,3]

[1]College of Communications Engineering, PLA University of Science and Technology, Nanjing 210007, China
[2]Centre for Quantum Technologies, National University of Singapore, Singapore
[3]Centre for Quantum Computation and Communication Technology, Department of Quantum Science, The Australian National University, Canberra, ACT 0200, Australia

Abstract

We present a novel approach called the intermediate rotating wave approximation (IRWA), which employs a time-averaging method to encapsulate the dynamics of light-matter interaction from strong to ultrastrong coupling regime. In contrast to the ordinary rotating wave approximation, this method addresses the co-rotating and counter-rotating terms separately to trace their physical consequences individually, and thus establishes the continuity between the Jaynes-Cummings model and the quantum Rabi model. We investigate IRWA in near resonance and large detuning cases. Our IRWA not only agrees well with both models in their respective coupling strengths, but also offers a good explanation for their differences.

Keywords: Ultrastrong coupling regime, Jaynes-Cummings model, Rabi model, Intermediate rotating wave approximation.
PACS: 42.50.Pq, 42.50.Ct, 42.50.-p

1. Introduction

The quantum Rabi model (QRM), which describes the interaction between a qubit and a quantized harmonic oscillator (bosonic mode) [1], is written as

$$H_{Rabi} = \frac{1}{2}\hbar\omega_a\sigma_z + \hbar\omega_r a^\dagger a + \hbar g\sigma_x(a + a^\dagger), \quad (1)$$

where a ($a^\dagger$) represents the bosonic annihilation (creation) operator of the electromagnetic field mode, ω_r is the corresponding frequency; ω_a is the transition frequency of the qubit, σ_i ($i = x, y, z$) are the corresponding Pauli operators; and g is the dipole interaction strength. The QRM has been widely applied in modern physics, ranging from condensed-matter physics [2], atomic physics [3] to quantum optics [4], such as cavity QED [5] and circuit QED [6, 7] systems. Given its great importance, the QRM has been studied extensively using various methods [8, 9]. Despite all those studies, the exact solution of QRM was only obtained by Braak recently [10]. This analytical solution, however, is in the form of composite transcendental function defined in power series. The search for simpler analytical solution of generalized QRM with more physical insights thus continued [11, 12]. For example, the Bogoliubov-type transformation [13, 14, 15] is used to diagonalize the Hamiltonian to gain solutions and properties of the model [16, 17].

The quantum Rabi model can be further simplified into the renowned Jaynes-Cummings model (JCM) [18] by rotating wave approximation (RWA) provided that the coupling strength is sufficiently weak ($g \ll \min\{\omega_r, \omega_a\}$), and the detuning is small enough ($|\omega_a - \omega_r| \ll \omega_r + \omega_a$). In the interaction picture, the rotating terms $\sigma_+ a$ and $\sigma_- a^\dagger$ oscillate slowly with phase factor of $\exp[\pm i(\omega_a - \omega_r)t]$, whereas the two "counter-rotating" terms $\sigma_+ a^\dagger$ and $\sigma_- a$ oscillate rapidly with phase factor of $\exp[\pm i(\omega_r + \omega_a)t]$. Together with weak coupling condition, one can separate the time scales and discard the fast-oscillating terms [4, 19, p.354], thus obtaining the Jaynes-Cummings Hamiltonian

$$H_{JC} = \frac{1}{2}\hbar\omega_a\sigma_z + \hbar\omega_r a^\dagger a + \hbar g(\sigma_+ a + \sigma_- a^\dagger), \quad (2)$$

which has simple analytical solutions.

Enhancement and tunability of light-matter interaction is crucial not only for fundamental studies of cavity/circuit QED but also for their applications

in quantum information processing. Three different coupling regimes can be defined based on the basic frequency scales of the system. In the weak coupling regime ($g \ll \{\gamma, \kappa\}$, κ and γ being the loss rate of the photon and the emitters' excitation), the discrete density of photonic states modifies the radiative lifetime of the quantum emitters (Purcell effect) [20]. Strong coupling regime is achieved when $\{\gamma, \kappa\} \ll g \ll \min\{\omega_r, \omega_a\}$ [21, p.432], such that quantum emitters absorb and spontaneously re-emit a photon many times before dissipation becomes effective. This strong coupling regime has been investigated in various systems, ranging from atoms [5], through quantum dots (QD) [22] to Cooper-pair boxes [6]. In these conventional QED experiments, the system is operating in either weak coupling regime or strong coupling regime. Therefore, the RWA, which leads to JCM from QRM, is very well justified, and the JCM captures a wealth of physical phenomena in conventional QED systems comprehensively. With recent advances of new technologies, the ultrastrong coupling regime has become experimentally accessible in semiconductor [23, 24, 25] and superconducting systems [7, 26]. In this so-called ultrastrong coupling regime [27], the coupling strength becomes comparable to the frequency of the resonator, $g/\omega_r \gtrsim 0.1$. Therefore, the routinely invoked RWA and the JCM break down, and the systems dynamics become governed by the QRM. This novel unexplored physics has opened up new research interest in applications of the QRM. Since then, considerable progress has been made and fascinating phenomenon have been predicted, such as photon blockade [28], nonclassical state generation [29], breakdown of the standard master equation [30], and ultrafast two-qubit quantum gate operations [31].

One interesting observation is that the co-rotating terms and counter-rotating terms in the QRM affect the system in a different manner depending on the coupling regime. In light of this, one could gain better physical intuition of the continuity between the JCM and the QRM by treating the coupling strength of the co-rotating terms and counter-rotating terms separately [32, 33]. In this paper, we seek to understand the emergence of the counter-rotating terms from the JCM to the QRM by resorting to the time-averaging method [4, p. 353], which also helps us to keep track of the time scale involved in the dynamics. With this method, we deploy a form of approximation, which we term as intermediate RWA (IRWA). The basic idea of this approximation is that, instead of going to the limit of either RWA or non-RWA, we use the time-averaged coupling strength in the interaction Hamiltonian. We present the general formalism and apply the IRWA into two specific situations: the near resonance case and the dispersive (large detuning) case.

The paper is organized as follows. In Sec. 2, we first give a brief review of the time-averaging approach and introduce the IRWA. In Sec. 3, the IRWA is used to study the energy levels of the system by perturbation theory in the near resonance case with increasing coupling strength. In Sec. 4, the dynamics of the system is investigated in the dispersive case with IRWA for both single- and multi-qubit case. We summarize our results in Sec. 5.

2. Time-averaging and intermediate RWA

2.1. Time-averaging function

The slow and fast time scales in a dynamical system can be separated explicitly by means of a temporal filtering operation. The time average of a function is defined by the convolution

$$\overline{f(t)} = \int_{-\infty}^{\infty} dt' \varpi(t-t') f(t') = \int_{-\infty}^{\infty} dt' \varpi(t') f(t+t'), \quad (3)$$

where the averaging function $\varpi(t)$ is positive, $\varpi(t) \geq 0$, even, $\varpi(t) = \varpi(-t)$, and normalized, $\int_{-\infty}^{\infty} dt\, \varpi(t) = 1$ [4, p.353]. The weighting function $\varpi(t)$ has a temporal width $\tau = \left[\int_{-\infty}^{\infty} \mathrm{d}t \varpi(t)\, t^2\right]^{1/2} < \infty$, which washes out oscillation with period smaller than τ.

A simple example of such function is a Gaussian function

$$\varpi(t) = \frac{1}{\tau\sqrt{2\pi}}\, e^{-\frac{t^2}{2\tau^2}}. \quad (4)$$

It is more convenient to work in the domain of frequency, by using the Fourier transformed time-averaging function,

$$K(\omega) = \int_{-\infty}^{\infty} dt\, \varpi(t) e^{i\omega t}, \quad (5)$$

which is real and even, $K(-\omega) = K(\omega) = K^*(\omega)$, and has a finite width of $\omega_K \approx 1/\tau$. The Fourier transform of the convolution Eq.(3) is just the product of the individual Fourier transforms:

$$\overline{F(\omega)} = K(\omega) F(\omega). \quad (6)$$

$K(\omega)$ is also called the cut-off function, which acts on $F(\omega)$ in such a way that $F(\omega)$ is essentially unchanged for small frequencies, $\omega \ll \omega_K$, whereas frequencies larger than the width $\omega \gg \omega_K$ are strongly suppressed.

2.2. Time-averaged Hamiltonian in intermediate RWA

In order to apply the time-averaging function to the QRM, we impose the condition

$$g \ll \omega_K \tag{7}$$

where the cut-off frequency ω_K is chosen in such a way that the state interaction-picture state $|\psi(t)\rangle$ is essentially constant over the averaging interval, i.e. $|\psi(t)\rangle \approx \overline{|\psi(t)\rangle}$. Upon time-averaging, the Schrödinger equation of the QRM in the interaction picture can be written as [4, p. 354]

$$i\hbar\frac{\partial}{\partial t}|\psi(t)\rangle = \overline{H}_{int}|\psi(t)\rangle, \tag{8}$$

where time-averaged Hamiltonian $\overline{H}_{int}(t)$ reads

$$\overline{H}_{int}(t) = \overline{H}_{int,r}(t) + \overline{H}_{int,ar}(t), \tag{9}$$

$$\overline{H}_{int,r}(t) = \hbar g_r\left(a\sigma_+ e^{i\Delta t} + a^\dagger\sigma_- e^{-i\Delta t}\right), \tag{10}$$

$$\overline{H}_{int,ar}(t) = \hbar g_{ar}\left(a\sigma_- e^{-i\Sigma t} + a^\dagger\sigma_+ e^{i\Sigma t}\right). \tag{11}$$

Here, the time-averaged coupling strengths for co-rotating term g_r and for counter-rotating term g_{ar}, are modified by the cut-off functions, such that $g_r = K(\pm\Delta)g$ and $g_{ar} = K(\pm\Sigma)g$, with $\Delta = \omega_a - \omega_r$ and $\Sigma = \omega_a + \omega_r$. This guarantees that the co-rotating terms $\sigma_+ a$, $\sigma_- a^\dagger$ and the counter-rotating terms $\sigma_+ a^\dagger$, $\sigma_- a$ contribute differently to the dynamics of the system, depending on the separation of the frequency scales. Notice that since the cut-off frequency ω_K is coupling strength dependent (c.f. Eq.(7)), the cut-off function $K(\omega)$ thus is a function of both g and ω, i.e. $K(\omega, \omega_K(g))$.

Going back to Schrödinger picture, we then have the time-averaged quantum Rabi model as

$$\overline{H}_{Rabi} = H_0 + \overline{H}_r + \overline{H}_{ar}, \tag{12}$$

where

$$\overline{H}_r = \hbar g_r X_+, \qquad \text{with} \qquad X_\pm = a\sigma_+ \pm a^\dagger\sigma_-; \tag{13}$$

$$\overline{H}_{ar} = \hbar g_{ar} Y_+, \qquad \text{with} \qquad Y_\pm = a\sigma_- \pm a^\dagger\sigma_+. \tag{14}$$

The condition of $|\Delta| \leq \Sigma$ is generally satisfied in cavity/circuit QED systems, but this does not give a justification for us to neglect the contribution of the counter-rotating Hamiltonian $\overline{H}_{ar}$, and the QRM is still needed to describe the system. In the case of RWA, the sufficiently weak coupling condition, $g \ll \min\{\omega_r, \omega_a\}$, allows us to separate the frequency scales by

$$g \ll \omega_K \ll \min\{\omega_r, \omega_a\} \leq \Sigma. \tag{15}$$

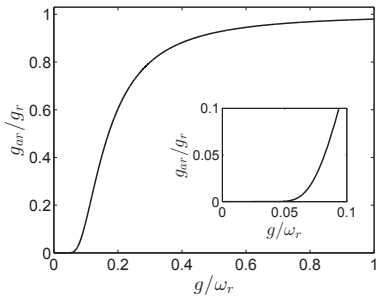

Figure 1: The ratio of the time-averaged coupling strengths g_{ar} for counter-rotating terms to g_r for co-rotating terms as a function of coupling strength g/ω_r, with Gaussian weighting function of width $\omega_K = 10g$ for small detuning, $\Delta = 0.01\omega_r$. As the coupling strength is further increased, even though the near resonance condition is satisfied, the weak coupling condition is no longer respected and hence, RWA is not applicable any longer. The inset is a zoom of the region of g/ω_r between 0 and 0.1.

Therefore, when the coupling strength is weak compared to the free energy of the system, counter-rotating contribution is negligible since the cut-off function $K(\Sigma)$ is vanishingly small. In Fig. 1, we show the ratio between the two time-averaged coupling strengths g_{ar} and g_r as a function of the normalized coupling strength g/ω_r, with Gaussian weighting function of width $\omega_K = 10g$ for small qubit-resonator detuning $\Delta = 0.01\omega_r$. We note that, with small coupling strength, i.e. $g/\omega_r \lesssim 0.05$, the time-averaged coupling strength g_{ar} for counter-rotating terms is negligible for small detuning, which agrees well with the RWA conditions. We then arrive at the time-averaged JCM in Schrödinger picture,

$$\overline{H}_{JC} = \frac{1}{2}\hbar\omega_a\sigma_z + \hbar\omega_r a^\dagger a + \hbar g_r X_+. \tag{16}$$

However, as the coupling strength is getting larger, the contribution of the counter-rotating terms is increasing and hence, needs to be included to describe the dynamics correctly.

3. Near resonance case in intermediate RWA

In the near resonance case of $|\Delta| \ll \min\{\omega_a, \omega_r\} \ll \omega_a + \omega_r$, the time-averaged coupling strength for counter-rotating terms is much smaller than the time-averaged coupling strength for co-rotating terms, $g_{ar} \ll g_r$. Thus, we take the time-averaged counter-rotating Hamiltonian in Eq.(14) as a perturbation to the time-averaged Jaynes-Cummings Hamiltonian in Eq.(16) and apply the non-degenerate stationary perturbation theory to obtain the

second-order modification for energy [34, p.249]. The results can be written as

$$E_{0,g} = E^{(0)}_{0,g} + E^{(1)}_{0,g} + E^{(2)}_{0,g}, \tag{17}$$

$$E_{n,\pm} = E^{(0)}_{n,\pm} + E^{(1)}_{n,\pm} + E^{(2)}_{n,\pm}, \quad (n = 1, 2, 3...), \tag{18}$$

where

$$E^{(0)}_{0,g} = -\frac{1}{2}\hbar\omega_a, \tag{19}$$

$$E^{(0)}_{n,\pm} = \left(n + \frac{1}{2}\right)\hbar\omega_r \pm \frac{1}{2}\hbar\sqrt{\Delta^2 + 4g_r^2(n+1)}, \tag{20}$$

$$E^{(1)}_{0,g} = E^{(1)}_{n,\pm} = 0, \tag{21}$$

and

$$E^{(2)}_{0,g} = |\hbar g_{ar}|^2 \left(\frac{|C_1|^2}{E^{(0)}_{0,g} - E^{(0)}_{1,+}} + \frac{|S_1|^2}{E^{(0)}_{0,g} - E^{(0)}_{1,-}}\right), \tag{22}$$

$$E^{(2)}_{0,+} = 2\,|\hbar g_{ar} S_0|^2 \left(\frac{|C_2|^2}{E^{(0)}_{0,+} - E^{(0)}_{2,+}} + \frac{|S_2|^2}{E^{(0)}_{0,+} - E^{(0)}_{2,-}}\right), \tag{23}$$

$$E^{(2)}_{0,-} = 2\,|\hbar g_{ar} C_0|^2 \left(\frac{|C_2|^2}{E^{(0)}_{0,-} - E^{(0)}_{2,+}} + \frac{|S_2|^2}{E^{(0)}_{0,-} - E^{(0)}_{2,-}}\right), \tag{24}$$

$$E^{(2)}_{1,+} = \frac{|\hbar g_{ar} C_1|^2}{E^{(0)}_{1,+} - E^{(0)}_{0,g}} + 3\,|\hbar g_{ar} S_1|^2 \left(\frac{|C_3|^2}{E^{(0)}_{1,+} - E^{(0)}_{3,+}} + \frac{|S_3|^2}{E^{(0)}_{1,+} - E^{(0)}_{3,-}}\right), \tag{25}$$

$$E^{(2)}_{1,-} = \frac{|\hbar g_{ar} S_1|^2}{E^{(0)}_{1,-} - E^{(0)}_{0,g}} + 3\,|\hbar g_{ar} C_1|^2 \left(\frac{|C_3|^2}{E^{(0)}_{1,-} - E^{(0)}_{3,+}} + \frac{|S_3|^2}{E^{(0)}_{1,-} - E^{(0)}_{3,-}}\right), \tag{26}$$

$$E^{(2)}_{n\geq 2,+} = n\,|\hbar g_{ar} C_n|^2 \left(\frac{|S_{n-2}|^2}{E^{(0)}_{n,+} - E^{(0)}_{n-2,+}} + \frac{|C_{n-2}|^2}{E^{(0)}_{n,+} - E^{(0)}_{n-2,-}}\right) + (n+2)\,|\hbar g_{ar} S_n|^2 \left(\frac{|C_{n+2}|^2}{E^{(0)}_{n,+} - E^{(0)}_{n+2,+}} + \frac{|S_{n+2}|^2}{E^{(0)}_{n,+} - E^{(0)}_{n+2,-}}\right), \tag{27}$$

$$E^{(2)}_{n\geq 2,-} = n\,|\hbar g_{ar} S_n|^2 \left(\frac{|S_{n-2}|^2}{E^{(0)}_{n,-} - E^{(0)}_{n-2,+}} + \frac{|C_{n-2}|^2}{E^{(0)}_{n,-} - E^{(0)}_{n-2,-}}\right) + (n+2)\,|\hbar g_{ar} C_n|^2 \left(\frac{|C_{n+2}|^2}{E^{(0)}_{n,-} - E^{(0)}_{n+2,+}} + \frac{|S_{n+2}|^2}{E^{(0)}_{n,-} - E^{(0)}_{n+2,-}}\right), \tag{28}$$

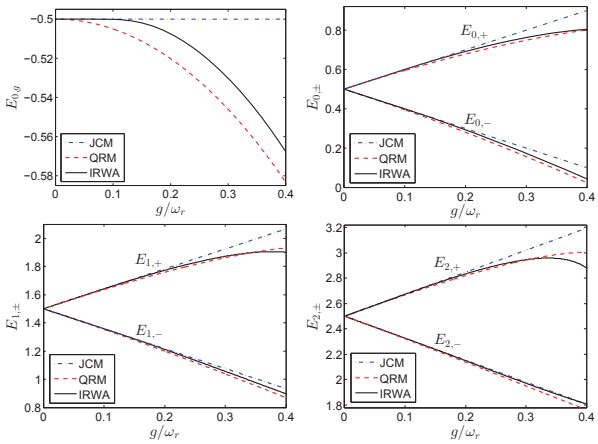

Figure 2: (Color online) The system spectrum as a function of the coupling strength g/ω_r with the time-averaged counter-rotating Hamiltonian of the IRWA in second perturbation theory (black solid lines) compared to the JCM (blue dashed-dotted lines) and the QRM (red dashed lines) for $\Delta = 0$ and $\omega_K = 10g$.

with $C_n = \cos\theta_n$, $S_n = \sin\theta_n$, and $\theta_n = \arctan(2g_r\sqrt{n+1}/\Delta)$.

The eigenenergies of the ground and low-lying excited states as a function of coupling strength g/ω_r are plotted in Fig. 2, which are obtained by our approach of IRWA (black solid lines), the JCM (blue dashed-dotted lines) and the QRM (red dashed lines). As shown in figure Fig. 2, the JCM curves deviate from the QRM curves for increasing coupling strength. The curves of the second-order perturbation theory in IRWA agree with the numerical results of the QRM for ultrastrong coupling regime of g/ω_r up to about 0.3.

4. Dispersive case in intermediate RWA

In this section, we will study the dynamics of the Rabi Hamiltonian in the dispersive limit, where the qubit and the resonator are far detuned compared to the coupling strength $g \ll |\Delta|$. The dispersive regime is of practical interests with applications in many cavity/circuit QED systems, such as quantum non-demolition measurement of the qubit [35], parity measurement of the two- or multi-qubit state [36], and quantum gate operations [37]. However, most of these applications were studied under the condition of strong coupling regime, where RWA still holds. In 2009, Zueco et al. generalized the studies of dispersive Hamiltonian to the ultrastrong coupling regime [19]. Although the effect of counter-rotating terms is merely quantitative in single qubit case, the treatment beyond RWA gives rise to a qualitatively different effective model for multi-qubit scenario. Using

the time-averaging functions in Sec. 2 to keep track of both the co-rotating and counter-rotating terms in the Hamiltonian, we can gain a better insight of their contributions and hence, the transition from the JCM to the QRM.

4.1. Dispersive Regime in One Qubit

In the dispersive limit, where the coupling strength is much lesser than the qubit-resonator detuning,

$$g \ll |\Delta|\,, \tag{29}$$

the time-averaged QRM in Eq.(12) can be transformed to

$$\begin{aligned} H_{ir}^{d} =& U\overline{H}_{Rabi}U^{\dagger} \\ \approx& \frac{\hbar}{2}\omega_a\sigma_z + \hbar\omega_r a^{\dagger}a + \frac{\hbar}{2}\left(\frac{g_r^2}{\Delta} + \frac{g_{ar}^2}{\Sigma}\right)\left[\sigma_z\left(2a^{\dagger}a+1\right)\right] \\ &+ \frac{\hbar}{2}g_r g_{ar}\left(\frac{1}{\Delta}+\frac{1}{\Sigma}\right)\left[\sigma_z\left(a^{\dagger 2}+a^2\right)\right], \end{aligned} \tag{30}$$

up to second order in $\lambda = g_r/\Delta$ and $\Lambda = g_{ar}/\Sigma$ via the unitary transformation [19, 38],

$$U = \exp[\lambda X_- + \Lambda Y_-]. \tag{31}$$

X_- and Y_- are defined in Eq.(13) and Eq.(14). In strong coupling regime with RWA, we have the following inequalities

$$g \ll |\Delta| \ll \omega_K \ll \Sigma, \tag{32}$$

which encapsulate the dispersive limit and the RWA conditions (near resonance and weak coupling limit) while respecting the time-averaging condition Eq.(7). When these inequalities are satisfied such that $g_{ar} \simeq 0$, $g_r = g$, the counter-rotating terms can be safely discarded. This gives rise to

$$H_r^d = \frac{\hbar}{2}\left(\omega_a + \frac{g^2}{\Delta}\right)\sigma_z + \hbar\left(\omega_r + \frac{g^2}{\Delta}\sigma_z\right)a^{\dagger}a, \tag{33}$$

where the oscillator frequency is shifted as

$$\omega_r \to \omega_{r,r} = \omega_r \pm g^2/\Delta, \tag{34}$$

depending on the state of the qubit. Similarly, the level separation of the qubit is shifted to

$$\omega_a \to \omega_{a,r} = \omega_a + \left(\frac{g^2}{\Delta} + 2\frac{g^2}{\Delta}a^{\dagger}a\right), \tag{35}$$

depends on the number of photons in the resonator. The term $2a^{\dagger}ag^2/\Delta$, which is linear in the mean photon number $n = \langle a^{\dagger}a\rangle$, is the ac-Stark shift [6] and g^2/Δ is the Lamb shift [19, 39]. On the other hand, given the fact that the resulting Hamiltonian H_r^d commutes with σ_z, i.e. $[H_r^d, \sigma_z] = 0$, it allows quantum non-demolition measurement since the qubit's state will not be changed upon the evolution of the system. Hence, the state of the qubit can be inferred by probing the resonator frequency.

In ultrastrong coupling regime, where either or both of the RWA conditions are violated, we have the following inequalites instead,

$$g \ll |\Delta| \leq \Sigma \ll \omega_K, \tag{36}$$

and all terms in Eq.(30) will be retained, and the effective Hamiltonian then reads

$$H_{nr}^d = \frac{\hbar}{2}\omega_a\sigma_z + \hbar\left[\omega_r + \frac{g^2}{2}\left(\frac{1}{\Delta}+\frac{1}{\Sigma}\right)\sigma_z\right]\left(a+a^{\dagger}\right)^2. \tag{37}$$

This expression is analogous to the RWA dispersive Hamiltonian in Eq.(33), with an extra contribution of Σ in the coupling term. However, this Hamiltonian is not diagonal in the eigenbasis of H_0 due to $a^{\dagger 2}$ and a^2. Nevertheless, for $g/\omega_r < 1$, we can reinterpret the result as the state-dependent shift of the resonator frequency's potential curvature ω_r^2 [19]. Hence, the dispersive Hamiltonian with non-RWA gives rise to a shift in the oscillator frequency of

$$\omega_r \to \omega_{r,nr} = \omega_r \pm g^2\left(\frac{1}{\Delta}+\frac{1}{\Sigma}\right), \tag{38}$$

which implies that dispersive readout is also possible even in the ultrastrong coupling regime. Looking back at Eq.(30), we notice that both the time-averaged coupling strength g_{ar} and g_{ar} contribute to the two-photons terms $a^{\dagger 2}$ and a^2 in the Hamiltonian. The time average coupling strength associated with counter-rotating terms also leads to an extra qubit dependent shift $g^2\sigma_z/\Delta$.

Next, we study dynamics of the dispersive case from strong coupling regime to ultrastrong coupling regime use the time-averaged coupling strength in IRWA by numerical simulation. In Fig. 3, we show the frequency shift of the resonator as a function of normalized coupling strength g/ω_r for positive detuning $\Delta > 0$ and negative detuning $\Delta < 0$ in RWA (blue dashed-dotted lines), non-RWA (red dashed lines) and IRWA (black solid lines) with Gaussian weighting function. It is clear that the RWA results have a totally different trend compared with the non-RWA

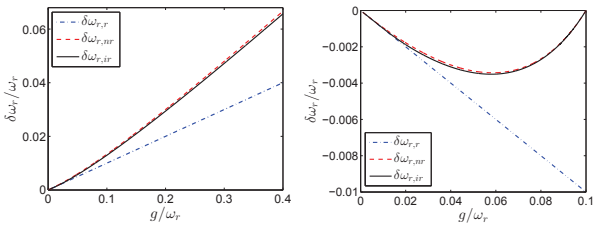

Figure 3: (Color online) Resonator frequency shift with single qubit in dispersive case as a function of coupling strength g/ω_r obtained with RWA (blue dashed-dotted lines), non-RWA (red dashed lines) and IRWA (black solid lines) for (a) positive detuning $\Delta > 0$ ($\Delta = 10g$) and (b) negative detuning $\Delta < 0$ ($\Delta = -10g$) with Gaussian weighting function of width $\omega_K = 10|\Delta|$. The breakdown of RWA is obvious, where it underestimates the dispersive shift for positive detuning and gives rise to a spurious shift in the absence of qubit ($\omega_a = 0$) for negative detuning.

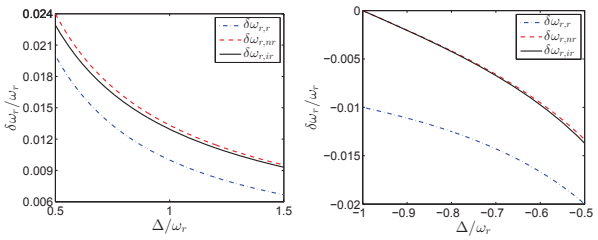

Figure 4: (Color online) Resonator frequency shift with single qubit in dispersive case as a function of detuning Δ/ω_r obtained with RWA (blue dashed-dotted lines), non-RWA (red dashed lines) and IRWA (black solid lines) for (a) positive detuning $\Delta > 0$ and (b) negative $\Delta < 0$ with Gaussian weighting function of width $\omega_K = 10|\Delta|$ and $g/\omega_r = 0.1$.

results, especially for larger coupling strength. It underestimates the dispersive shift for positive detuning and predicts a shift even when the qubit's frequency ω_a tends to be zero for negative detuning ($\Delta \to \omega_r$ as g increases). This indicates the breakdown of RWA in predicting the dispersive resonator frequency shift in ultrastrong coupling regime. Meanwhile, our IRWA shows the manifestation of the counter-rotating terms as the coupling strength increases.

In Fig. 4, we show the frequency shift of the resonator as a function of detuning Δ/ω_r in RWA (blue dashed-dotted lines), non-RWA (red dashed lines) and IRWA (black solid lines) with coupling strength of $g/\omega_r = 0.1$ and Gaussian weighting function of width $\omega_K = 10|\Delta|$. For this relatively large coupling strength, it is shown that the RWA results underestimate the resonator frequency shift for JCM, whereas the IRWA predictions agree quite well with the non-RWA results for QRM.

4.2. Dispersive Regime with multi-qubit

We now extend our discussion to multiple qubits coupled to a single mode resonator, where the time-averaged Hamiltonian takes the form [40]

$$\overline{H}^{nq}_{Rabi} = \frac{\hbar}{2}\sum_j \omega_a^j \sigma_z^j + \hbar\omega_r a^\dagger a + \hbar\sum_j \left(g_r^j X_+^j + g_{ar}^j Y_+^j\right), \tag{39}$$

with $X_\pm^j = a\sigma_+^j \pm a^\dagger\sigma_-^j$ and $Y_\pm^j = a\sigma_-^j \pm a^\dagger\sigma_+^j$. Applying the unitary transformation

$$U^{nq} = \exp\left(\sum_j \left(\lambda_j X_-^j + \Lambda_j Y_-^j\right)\right), \tag{40}$$

and expanding the transformed Hamiltonian to the second order in λ_j and Λ_j, we obtain the dispersive Hamiltonian

$$\begin{aligned} H_{ir}^{2q,d} =& \hbar\omega_r a^\dagger a + \frac{\hbar}{2}\sum_j \omega_a^j \sigma_z^j \\ &+ \frac{\hbar}{2}\sum_j \left(\frac{(g_r^j)^2}{\Delta_j} + \frac{(g_{ar}^j)^2}{\Sigma_j}\right)\left[\sigma_z^j\left(2a^\dagger a + 1\right)\right] \\ &+ \frac{\hbar}{2}\sum_{j>k} g_r^j g_r^k \left(\frac{1}{\Delta_j} + \frac{1}{\Delta_k}\right)\left(\sigma_-^j\sigma_+^k + \sigma_+^j\sigma_-^k\right) \\ &- \frac{\hbar}{2}\sum_{j>k} g_{ar}^j g_{ar}^k \left(\frac{1}{\Sigma_j} + \frac{1}{\Sigma_k}\right)\left(\sigma_-^j\sigma_+^k + \sigma_+^j\sigma_-^k\right) \\ &+ \frac{\hbar}{2}\sum_{j>k} g_r^j g_{ar}^k \left(\frac{1}{\Delta_j} - \frac{1}{\Sigma_k}\right)\left(\sigma_-^j\sigma_-^k + \sigma_+^j\sigma_+^k\right) \\ &+ \frac{\hbar}{2}\sum_{j>k} g_{ar}^j g_r^k \left(\frac{1}{\Delta_k} - \frac{1}{\Sigma_j}\right)\Big]\left(\sigma_-^j\sigma_-^k + \sigma_+^j\sigma_+^k\right), \end{aligned} \tag{41}$$

where the last four terms are the effective coupling between the qubits mediated by the resonator.

To illustrate, we now take a two-qubit system as an example. In RWA, the counter-rotating terms are discarded because $g_{ar}^{j,k} \approx 0$. By setting all $g_r^j = g$ and $\omega_a^j = \omega_a$, we obtain

$$\begin{aligned} H_r^{2q,d} =& \frac{\hbar}{2}\sum_j \left(\omega_a^j + \frac{g^2}{\Delta}\right)\sigma_z^j + \hbar\sum_j \left(\omega_r + \frac{g^2}{\Delta}\sigma_z^j\right)a^\dagger a \\ &+ \hbar\frac{g^2}{\Delta}\left(\sigma_-^j\sigma_+^k + \sigma_+^j\sigma_-^k\right), \end{aligned} \tag{42}$$

where the interqubit interaction is of isotropic XY type, $\sigma_-^j\sigma_+^k + \sigma_+^j\sigma_-^k$. In a frame rotating at the qubit's

frequency, $H_r^{2q,d}$ generates the evolution

$$U_r^{2q,d} = \exp\left[-iJ_r t\left(a^\dagger a + \frac{1}{2}\right)\left(\sigma_z^j + \sigma_z^k\right)\right] \times \begin{pmatrix} 1 & 0 & 0 & 0 \\ 0 & \cos J_r t & i\sin J_r t & 0 \\ 0 & i\sin J_r t & \cos J_r t & 0 \\ 0 & 0 & 0 & 1 \end{pmatrix} \otimes I_r \tag{43}$$

with I_r being the identity operator in resonator space and the effective coupling strength being

$$J_r = \frac{g^2}{\Delta}. \tag{44}$$

This has been employed to generate qubit-qubit entanglement and quantum gate operations [6, 40]. For instance, by turning on the coupling for a period $t = \pi\Delta/4g^2$, we can generate a $\sqrt{i\text{SWAP}}$ gate which can be used to transform the state $\left|e_j, g_k\right\rangle$ into an entangled state $1/\sqrt{2}\left(\left|e_j, g_k\right\rangle + i\left|g_j, e_k\right\rangle\right)$. Here, $\left|e_j\right\rangle$ and $|g_k\rangle$ are the excited state for j-th qubit and ground state for the k-th qubit, respectively.

In ultrastrong coupling regime without RWA, all the terms will be retained. By setting all $g_r^j = g_{ar}^j = g$ and $\omega_a^j = \omega_a$ to be equal, we obtain

$$\begin{aligned} H_{nr}^{2q,d} &= \frac{\hbar}{2}\sum_j\left[\omega_a^j + g^2\left(\frac{1}{\Delta} + \frac{1}{\Sigma}\right)\right]\sigma_z^j \\ &+ \hbar g^2\left(\frac{1}{\Delta} - \frac{1}{\Sigma}\right)\sigma_x^j\sigma_x^k \\ &+ \hbar\sum_j\left[\omega_r + g^2\left(\frac{1}{\Delta} + \frac{1}{\Sigma}\right)\sigma_z^j\right]a^\dagger a, \end{aligned} \tag{45}$$

where the interqubit interaction is of Ising type $\sigma_x^j\sigma_x^k$. The evolution operator reads

$$U_{nr}^{2q,d} = \exp\left[-iJ_{nr,0}t\left(a^\dagger a + \frac{1}{2}\right)\left(\sigma_z^j + \sigma_z^k\right)\right] \times \begin{pmatrix} \cos J_{nr,1}t & 0 & 0 & i\sin J_{nr,1}t \\ 0 & \cos J_{nr,1}t & i\sin J_{nr,1}t & 0 \\ 0 & i\sin J_{nr,1}t & \cos J_{nr,1}t & 0 \\ i\sin J_{nr,1}t & 0 & 0 & \cos J_{nr,1}t \end{pmatrix} \otimes I_r, \tag{46}$$

in the frame rotating at the qubit's frequency with the effective coupling strength being

$$J_{nr,0} = g^2\left(\frac{1}{\Delta} + \frac{1}{\Sigma}\right), \tag{47}$$

$$J_{nr,1} = g^2\left(\frac{1}{\Delta} - \frac{1}{\Sigma}\right). \tag{48}$$

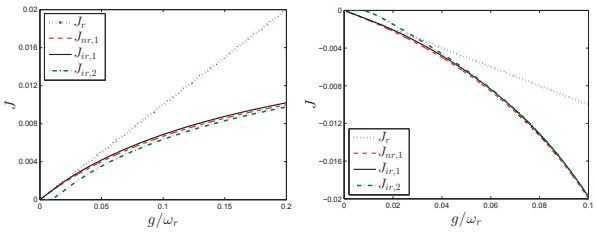

Figure 5: (Color online) The effective coupling strength in two-qubit dispersive case as a function of coupling strength g/ω_r obtained with RWA (blue dotted lines), non-RWA (red dashed lines) and IRWA (black solid lines and green dashed-dotted lines) for (a) positive detuning $\Delta > 0$ ($\Delta = 10g$) and (b) negative detuning $\Delta < 0$ ($\Delta = -10g$) with Gaussian weighting function of width $\omega_K = 10|\Delta|$.

It is worth noting that the extension from Eq.(42) to Eq.(45) is not just a renormalization of the parameters. The effective qubit-qubit interaction type is indeed different, which will be clearer when we compare the evolution operators for RWA and non-RWA (Eq.(43) and Eq.(46)), where one is isotropic XY interaction while the other is Ising type interaction respectively. To understand this apparent sudden transition between RWA and non-RWA in dispersive regime for the multi-qubit, we invoke the time-averaged IRWA interpretation. From the effective Hamiltonian in Eq.(41), the evolution operator can be written as

$$U_{ir}^{2q,d} = \exp\left[-iJ_{ir,0}t\left(a^\dagger a + \frac{1}{2}\right)\left(\sigma_z^j + \sigma_z^k\right)\right] \times \begin{pmatrix} \cos J_{ir,2}t & 0 & 0 & i\sin J_{ir,2}t \\ 0 & \cos J_{ir,1}t & i\sin J_{ir,1}t & 0 \\ 0 & i\sin J_{ir,1}t & \cos J_{ir,1}t & 0 \\ i\sin J_{ir,2}t & 0 & 0 & \cos J_{ir,2}t \end{pmatrix} \otimes I_r, \tag{49}$$

where the effective coupling strengths being

$$J_{ir,0} = \frac{\left(g_r^j\right)^2}{\Delta_j} + \frac{\left(g_{ar}^j\right)^2}{\Sigma_j}, \tag{50}$$

$$J_{ir,1} = g_r^j g_r^k\left(\frac{1}{\Delta_j} + \frac{1}{\Delta_k}\right) - g_{ar}^j g_{ar}^k\left(\frac{1}{\Sigma_j} + \frac{1}{\Sigma_k}\right), \tag{51}$$

$$J_{ir,2} = g_r^j g_{ar}^k\left(\frac{1}{\Delta_j} - \frac{1}{\Sigma_k}\right) + g_{ar}^j g_r^k\left(\frac{1}{\Delta_k} - \frac{1}{\Sigma_j}\right). \tag{52}$$

In Fig. 5, we show the transition of the difference for the qubit-qubit interaction type from RWA case to non-RWA using the IRWA with Gaussian weighting function of width $\omega_K = 10|\Delta|$. As we can see, when the coupling strength is very small, $g/\omega_r \ll 0.1$, the IRWA curves are closer to the RWA curves for $J_{ir,1}$, whereas they are essentially zero for $J_{ir,2}$. When the

coupling strength is increased, the counter-rotating term coupling strength g_{ar} starts to become significant, and hence, leads to the correction of $J_{ir,1}$ and manifestation of $J_{ir,2}$. As the coupling strength further increases, our IRWA curves start to deviate from the RWA curves and agree better with the non-RWA curves, showing the transitions from RWA to non-RWA. Eventually as the coupling strength reaches ultrastrong coupling regime, we regain the non-RWA results as in Eq. (46).

5. Conclusion

In this paper, we introduced the IRWA that is based on the time-averaging method for better understanding of the roles of the "counter-rotating" terms in the QRM and the transition between strong coupling and ultrastrong coupling regimes. The eigenenergies of the system were studied by combining the perturbation theory and IRWA for near resonance case. The results agreed well with the JCM predictions for small coupling strength, i.e. g/ω_r up to 0.1 and with the QRM results for larger coupling strength, i.e. g/ω_r up to 0.3. We also showed that in dispersive regime, our IRWA predication gave a good explanation of the qubit-dependent frequency shifts in the single qubit scenario. This approach revealed the emergence of counter-rotating terms in the interqubit coupling, which leads to both quantitative and qualitative differences in the interaction strength and interaction type. Compared with other approaches [11, 12, 16, 17], our IRWA method allows us to gain the physical consequences of the co-rotating and counter-rotating coupling terms individually by tracing those terms separately. As a remark, there are several aspects that still can be explored with the idea of IRWA. For instance, by relating the measurement interval to the width of the time-averaging function ω_K in our analysis, we can extend the result in [41] to observe the transition from quantum Zeno effect to quantum anti-Zeno effect [42, 43]. Our IRWA approach could also be applied to the studies of applicability of RWA in various phenomena, such as Berry phase in quantum systems [44, 45], asymmetric couplings [12], and generalized multi-qubit quantum Rabi model [32]. The IRWA might be useful as well in studying the dynamics of multiple coupling regimes in a single system, for example, by having one qubit coupled strongly in RWA regime and the other one operated ultrastrongly beyond RWA regime.

6. Acknowledgements

We acknowledge Valerio Scarani for his proposal of this research topic and valuable comments. We thank Tammy Chin for suggestions and feedback on the manuscript. This work was supported by Natural Science Foundation of Jiangsu Province (No. BK20140072) and National Natural Science Foundation of China (No. 11404407). J. Y. Haw would like to acknowledge the support of the Australian Research Council Centre of Excellence for Quantum Computation and Communication Technology (project number CE110001027).

References

[1] I. I. Rabi, Space Quantization in a Gyrating Magnetic Field, Physical Review 51 (8) (1937) 652–654.
[2] M. Wagner, Unitary Transformations in Solid State Physics, Elsevier Science Ltd, Amsterdam, 1986.
[3] C. Cohen-Tannoudji, J. Dupont-Roc, G. Grynberg, Atom-Photon Interactions, Wiley-VCH, Weinheim, 1998.
[4] J. Garrison, R. Chiao, Quantum Optics, Oxford University Press, Oxford, 2008.
[5] J. M. Raimond, M. Brune, S. Haroche, Manipulating quantum entanglement with atoms and photons in a cavity, Reviews of Modern Physics 73 (3) (2001) 565.
[6] A. Blais, R.-S. Huang, A. Wallraff, S. M. Girvin, R. J. Schoelkopf, Cavity quantum electrodynamics for superconducting electrical circuits: An architecture for quantum computation, Physical Review A 69 (6) (2004) 062320.
[7] T. Niemczyk, F. Deppe, H. Huebl, E. P. Menzel, F. Hocke, M. J. Schwarz, J. J. Garcia-Ripoll, D. Zueco, T. Hummer, E. Solano, A. Marx, R. Gross, Circuit quantum electrodynamics in the ultrastrong-coupling regime, Nature Physics 6 (10) (2010) 772–776.
[8] E. K. Irish, J. Gea-Banacloche, I. Martin, K. C. Schwab, Dynamics of a two-level system strongly coupled to a high-frequency quantum oscillator, Physical Review B 72 (19) (2005) 195410.
[9] E. K. Irish, Generalized Rotating-Wave Approximation for Arbitrarily Large Coupling, Physical Review Letters 99 (17) (2007) 173601.
[10] D. Braak, Integrability of the Rabi Model, Physical Review Letters 107 (10) (2011) 100401.
[11] H. Zhong, Q. Xie, M. T. Batchelor, C. Lee, Analytical eigenstates for the quantum Rabi model, Journal of Physics A: Mathematical and Theoretical 46 (41) (2013) 415302.
[12] J. Peng, Z. Ren, D. Braak, G. Guo, G. Ju, X. Zhang, X. Guo, Solution of the two-qubit quantum Rabi model and its exceptional eigenstates, Journal of Physics A: Mathematical and Theoretical 47 (26) (2014) 265303.
[13] E. Karpov, I. Prigogine, T. Petrosky, G. Pronko, Friedrichs model with virtual transitions. Exact solution and indirect spectroscopy, Journal of Mathematical Physics 41 (1) (2000) 118–131.
[14] G. Flores-Hidalgo, A. Malbouisson, Dressed-state approach to quantum systems, Physical Review A 66 (4) (2002) 042118.
[15] R. Passante, L. Rizzuto, S. Spagnolo, S. Tanaka, T. Petrosky, Harmonic oscillator model for the atom-surface Casimir-Polder interaction energy, Physical Review A 85 (6) (2012) 062109,

[16] Q.-H. Chen, C. Wang, S. He, T. Liu, K.-L. Wang, Exact solvability of the quantum Rabi model using Bogoliubov operators, Physical Review A 86 (2) (2012) 023822.
[17] J. Peng, Z. Ren, G. Guo, G. Ju, X. Guo, Exact solutions of the generalized two-photon and two-qubit Rabi models, The European Physical Journal D 67 (8) (2013) 1–9.
[18] E. T. Jaynes, F. W. Cummings, Comparison of quantum and semiclassical radiation theories with application to the beam maser, Proc. IEEE 51 (1963) 89–109.
[19] D. Zueco, G. M. Reuther, S. Kohler, P. Hanggi, Qubit-oscillator dynamics in the dispersive regime: Analytical theory beyond the rotating-wave approximation, Physical Review A 80 (3) (2009) 033846.
[20] E. Purcell, Spontaneous Emission Probabilities at Radio Frequencies, Physical Review 69 (11-1) (1946) 681–681.
[21] P. Meystre, M. Sargent, Elements of Quantum Optics, Springer, Berlin Heidelberg New York, 4th edn., 2007.
[22] G. Khitrova, H. M. Gibbs, M. Kira, S. W. Koch, A. Scherer, Vacuum Rabi splitting in semiconductors, Nature Physics 2 (2) (2006) 81–90.
[23] G. Gunter, A. A. Anappara, J. Hees, A. Sell, G. Biasiol, L. Sorba, S. D. Liberato, C. Ciuti, A. Tredicucci, A. Leitenstorfer, R. Huber, Sub-cycle switch-on of ultrastrong light-matter interaction, Nature 458 (7235) (2009) 178–181.
[24] M. Geiser, F. Castellano, G. Scalari, M. Beck, L. Nevou, J. Faist, Ultrastrong Coupling Regime and Plasmon Polaritons in Parabolic Semiconductor Quantum Wells, Physical Review Letters 108 (10) (2012) 106402.
[25] G. Scalari, C. Maissen, D. Turcinkova, D. Hagenmuller, S. D. Liberato, C. Ciuti, C. Reichl, D. Schuh, W. Wegscheider, M. Beck, J. Faist, Ultrastrong Coupling of the Cyclotron Transition of a 2D Electron Gas to a THz Metamaterial, Science 335 (6074) (2012) 1323–1326.
[26] P. Forn-Diaz, J. Lisenfeld, D. Marcos, J. J. Garcia-Ripoll, E. Solano, C. J. P. M. Harmans, J. E. Mooij, Observation of the Bloch-Siegert Shift in a Qubit-Oscillator System in the Ultrastrong Coupling Regime, Physical Review Letters 105 (23) (2010) 237001.
[27] J. Casanova, G. Romero, I. Lizuain, J. J. Garcia-Ripoll, E. Solano, Deep Strong Coupling Regime of the Jaynes-Cummings Model, Physical Review Letters 105 (26) (2010) 263603.
[28] A. Ridolfo, M. Leib, S. Savasta, M. J. Hartmann, Photon Blockade in the Ultrastrong Coupling Regime, Physical Review Letters 109 (19) (2012) 193602.
[29] S. Ashhab, F. Nori, Qubit-oscillator systems in the ultrastrong-coupling regime and their potential for preparing nonclassical states, Physical Review A 81 (4 (2010) 042311.
[30] F. Beaudoin, J. M. Gambetta, A. Blais, Dissipation and ultrastrong coupling in circuit QED, Physical Review A 84 (4) (2011) 043832.
[31] G. Romero, D. Ballester, Y. M. Wang, V. Scarani, E. Solano, Ultrafast Quantum Gates in Circuit QED, Physical Review Letters 108 (12) (2012) 120501.
[32] L.-T. Shen, Z.-B. Yang, R.-X. Chen, Ground state of three qubits coupled to a harmonic oscillator with ultrastrong coupling, Physical Review A 88 (4) (2013) 045803.
[33] F. T. Hioe, Phase Transitions in Some Generalized Dicke Models of Superradiance, Physical Review A 8 (3) (1973) 1440–1445.
[34] D. J. Griffiths, Introduction to Quantum Mechanics, Pearson Prentice Hall, New Jersey, 2nd edn., 2004.
[35] C. Guerlin, J. Bernu, S. Deleglise, C. Sayrin, S. Gleyzes, S. Kuhr, M. Brune, J.-M. Raimond, S. Haroche, Progressive field-state collapse and quantum non-demolition photon counting, Nature 448 (7156) (2007) 889–893.
[36] K. Lalumiere, J. M. Gambetta, A. Blais, Tunable joint measurements in the dispersive regime of cavity QED, Physical Review A 81 (4) (2010) 040301.
[37] J. Majer, J. M. Chow, J. M. Gambetta, J. Koch, B. R. Johnson, J. A. Schreier, L. Frunzio, D. I. Schuster, A. A. Houck, A. Wallraff, A. Blais, M. H. Devoret, S. M. Girvin, R. J. Schoelkopf, Coupling superconducting qubits via a cavity bus, Nature 449 (7161) (2007) 443–447.
[38] A. B. Klimov, S. M. Chumakov, A Group-Theoretical Approach to Quantum Optics: Models of Atom-Field Interactions, Wiley-VCH, Weinheim, 2009.
[39] A. Wallraff, D. I. Schuster, A. Blais, L. Frunzio, R.-S. Huang, J. Majer, S. Kumar, S. M. Girvin, R. J. Schoelkopf, Strong coupling of a single photon to a superconducting qubit using circuit quantum electrodynamics, Nature 431 (7005) (2004) 162–167.
[40] A. Blais, J. Gambetta, A. Wallraff, D. I. Schuster, S. M. Girvin, M. H. Devoret, R. J. Schoelkopf, Quantum-information processing with circuit quantum electrodynamics, Physical Review A 75 (3) (2007) 032329.
[41] I. Lizuain, J. Casanova, J. J. Garcia-Ripoll, J. G. Muga, E. Solano, Zeno physics in ultrastrong-coupling circuit QED, Physical Review A 81 (6) (2010) 062131.
[42] H. Zheng, S. Y. Zhu, M. S. Zubairy, Quantum Zeno and Anti-Zeno Effects: Without the Rotating-Wave Approximation, Physical Review Letters 101 (20) (2008) 200404.
[43] Q. Ai, Y. Li, H. Zheng, C. P. Sun, Quantum anti-Zeno effect without rotating wave approximation, Physical Review A 81 (4)(2010) 042116.
[44] J. Larson, Absence of Vacuum Induced Berry Phases without the Rotating Wave Approximation in Cavity QED, Physical Review Letters 108 (3) (2012) 033601.
[45] W.-W. Deng, G.-x. Li, Berry phase of the Rabi model beyond the rotating-wave approximation, Journal of Physics B: Atomic, Molecular and Optical Physics 46 (22) (2013) 224018.